energies

IMPACT FACTOR 3.0

CITESCORE 6.2

Article

Editor's Choice

A Nernst-Based Approach for Modeling of Lithium-Ion Batteries with Non-Flat Voltage Characteristics

Athar Ahmad, Mario Iamarino and Antonio D'Angola

MDPI

https://doi.org/10.3390/en17163914

energies

MDPI

Article

A Nernst-Based Approach for Modeling of Lithium-Ion Batteries with Non-Flat Voltage Characteristics

Athar Ahmad, Mario Iamarino and Antonio D'Angola *

Dipartimento di Ingegneria, Università degli Studi della Basilicata, 85100 Potenza, Italy; athar.ahmad@unibas.it (A.A.); mario.iamarino@unibas.it (M.I.)
* Correspondence: antonio.dangola@unibas.it

Abstract: This paper presents an easy-to-implement model to predict the voltage in a class of Li-ion batteries characterized by non-flat, gradually decreasing voltage versus capacity. The main application is for the accurate estimation of the battery state of the charge, as in the energy management systems of battery packs used in stationary and mobility applications. The model includes a limited number of parameters and is based on a simple equivalent circuit representation where an open circuit voltage source is connected in series with an equivalent resistance. The non-linear open circuit voltage is described using a Nernst-like term, and the model parameters are estimated based on the manufacturer discharge curves. The results show a good level of model accuracy in the case of three different commercial batteries considered by the study: Panasonic CGR18650AF, Panasonic NCR18650B and Tesla 4680. In particular, accurate description of the voltage curves versus the state of charge at different constant currents and during charging/discharging cycles is achieved. A possible model reduction is also addressed, and the effect of the equivalent internal resistance in improving the model predictions near fully depleted conditions is highlighted.

Keywords: Li-ion battery modeling; *SoC* prediction; Nernst equation; energy management system; CGR18650AF; NCR18650B; Tesla 4680

Citation: Ahmad, A.; Iamarino, M.; D'Angola, A. A Nernst-Based Approach for Modeling of Lithium-Ion Batteries with Non-Flat Voltage Characteristics. *Energies* **2024**, *17*, 3914. https://doi.org/10.3390/en17163914

Academic Editor: Carlos Miguel Costa

Received: 18 July 2024
Revised: 1 August 2024
Accepted: 2 August 2024
Published: 8 August 2024

1. Introduction

Energy storage in electrochemical batteries currently plays a vital role in both stationary renewable energy production and electric vehicle systems. Various technologies exist, including lead–acid, nickel–cadmium, nickel–metal hydrides, lithium-ion, etc., and the differences mainly lie in the materials used for the electrodes and the electrolyte, which determine energy density and other desired features. Over the past few decades, these systems have been the subject of significant enhancements in order to meet more and more challenging requirements. In this scenario, the lithium-ion batteries have demonstrated important advantages over other technologies due to their high density, low self-discharge and long life [1] and have been, therefore, the focus of an increasing number of scientific investigations aimed at improving performance and durability, as well as understanding the relevant underlying physical and chemical phenomena.

Within energy storage systems, the Li-ion battery is typically monitored and controlled by an energy management system (EMS), which ensures efficient and reliable operation. This is achieved by continuously assessing the current battery's conditions during operation, particularly by estimating key parameters such as the battery state of charge (*SoC*), state of health (*SoH*) and remaining useful life (*RUL*) [2]. In particular, the *SoC* is a measure of how much energy is available in the battery at any given moment and, therefore, plays a crucial role in the EMS, where it helps prevent over-charging and over-discharging, enhances user experience by providing information on available energy and improves the battery cycle life [3].

Since the *SoC* is a quantity that cannot be easily measured, and due to its crucial importance in real applications, many authors have developed various methods to estimate the *SoC*, each characterized by distinct levels of accuracy, complexity and the number of parameters involved [3,4]. Such methods can be classified in different groups [5]. Experiment-based methods involve an assessment of the cell dynamics and may include ampere integration methods, electrochemical impedance spectroscopy, etc. [6]. The data-driven methods involve compiling the available data on battery behavior and fitting them against measurements through various machine learning algorithms that rely on neural networks, regression or fuzzy logic approaches [7]. The multiple fusion methods are defined as the combination of model-based, experimental and data-driven methods, which helps improve the accuracy, as well as reduce computational time by learning from each other [8]. Finally, the model-based estimation methods typically consist of electrochemical models (EM), equivalent circuit models (ECM) or electrochemical impedance models (EIM) [9,10]. They rely on state equations and adaptive filters to estimate the internal behavior of the battery. In more detail, EM methods try to describe on a very microscopic level the relevant phenomena (charge transfer, reaction kinetics, etc.) and the spatial and temporal distribution of the related physical quantities (concentrations, potential, current, temperature, etc.) [11,12]. However, even after many simplifications, these models remain very complex and the parameters involved are numerous and difficult to quantify. The EIM models involve a deep analysis of the dynamic behavior of the battery through harmonic small-signal excitation, which allows for direct measurement of the voltage response at any operating point. They usually require high computational power, and the results are difficult to obtain in a short time. The ECM models have been widely used to describe the battery dynamics [13–18]. They represent the battery as an equivalent electrical circuit with resistors, capacitors and voltage sources suitably connected together in order to produce the actual terminal voltage of the battery [19]. This approach appears to be a good compromise between complexity and accuracy and typically allows for a quick estimation of the battery response under different loads, charging and discharging conditions, temperature, etc. [20,21]. Therefore, the modeling approach in this paper is based on the ECM concept, which requires, however, a good estimation of quantities such as the open circuit voltage and a proper description of the sources of energy dissipation.

During the recent decades, many authors have addressed the problem of accurately predicting the open circuit voltage of a Li-ion battery, and a number of different solutions have been proposed. Some of them rely on the complete knowledge of the composition and chemistry of the materials in the cell, which can be then described by thermodynamic equilibrium relationships, continuously adjusted to take into account the transfer of charges between cathode and anode. Very often, however, in the lack of a full characterization effort for the materials involved, the level of information available does not allow for such a detailed description. Alternatively, it is possible to resort to fully empirical correlations based on the observed voltage measurements, as in the example in [22], where a polynomial, an exponential, a sum of sin functions and a Gaussian model are tested in order to describe the open circuit voltage of a high-capacity Li-ion battery. These models, however, fail to explain the nature of the physical phenomena occurring inside the battery and, therefore, suffer from difficulties in generalization. As a good compromise, semi-empirical approaches, which try to some extent to keep a connection between model formulation and real phenomena, seem to have received particular attention. These mostly date back to the early work of C.M. Shepherd [23] on Li-ion batteries, with significant improvements achieved later by other authors in physical and numerical accuracy. In particular, this model has been further improved in [24,25] with the introduction of an additional non-linear term and a filtered current to address algebraic loop numerical issues and to better describe the battery fast dynamics. Due to its simplicity and the possibility to extract model parameters directly from the manufacturer's discharge curves without the need to apply non-linear optimization methods, one version of this approach has been also implemented and made publicly available in the Matlab/Simulink library [26], contributing further to

its popularity and widespread use in the scientific community [27,28]. The main idea behind Shepherd-like approaches is to build the voltage curve around a constant value, and these are, therefore, particularly suitable for modeling batteries with a main central voltage plateau, as is typical for LFP electrodes. Preliminary investigations by the authors and conclusions drawn from similar studies [29,30] indicate that these models are often less suitable for describing batteries that lack a clear main plateau, exhibiting instead a number of smaller plateaus or a smooth, gradually decreasing curve.

This paper tries to fill this gap by proposing an alternative model to address batteries without a clear voltage plateau, avoiding, at the same time, the over-complexity of a detailed description of solid state chemistry. The simplifications introduced allow us to resort to the classical Nernst equation to account for the continuous or quasi-continuous change in equilibrium potentials by means of a continuous function of the activities of the lithiated phases. The model presents a limited number of unknown parameters that can be easily estimated in the light of the typical discharging curves made available by battery manufacturers or from direct voltage measurements. The model is successfully applied to describe the voltage curves versus *SoC* for popular commercial batteries with cobalt-containing electrodes.

2. Mathematical Model

2.1. Theoretical Background

The operation of a Li-ion battery cell involves, unlike most other batteries, the intercalation of lithium ions between the layers of a suitable solid matrix, without significantly altering the original solid structure. In particular, during discharging, Li-ions deintercalate from the layered anodic material and migrate to intercalate between the layers of the cathodic material, and the opposite happens during charging. The resulting battery open circuit voltage is linearly related to the specific (per transferred ion and electron) Gibbs free energy change in the overall redox process according to the following expression:

$$V_{oc} = -\frac{\Delta g_r}{F} \tag{1}$$

where F is the Faraday constant (96,485 C mol^{-1}).

In some cases, the chemistry at a certain electrode involves a single lithiated phase and a single non-lithiated phase transforming into each other, without the formation of intermediate stages. This corresponds to a rather constant Δg_r of the corresponding semi-reaction due to the approximately invariant thermodynamic activities of these solids. The resulting electrode potential shows, therefore, a typical main plateau as in Figure 1a, measured versus an arbitrary standard electrode. Common cathode materials such as $LiFePO_4$ in the so-called LFP batteries fall in this category.

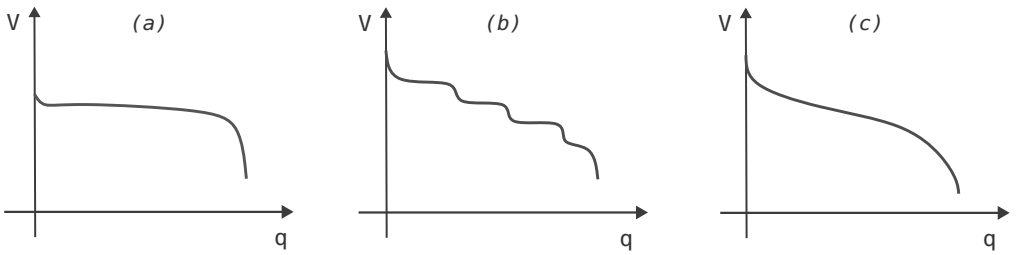

Figure 1. Possible shapes for the electrode potential during charging (anode) or discharging (cathode): (**a**) main plateau, (**b**) multiple plateaus and (**c**) smooth shape. Based on [31].

In other cases, the electrode can go through the formation of intermediate stable and meta-stable solid phases characterized by variable lithium content, creating a sequence of intermediate plateaus in the electrode potential, as in Figure 1b. A typical material falling in this category is the lithiated graphite, widely used as the anode in Li-ion batteries, where

the Li:C ratio in the intermediate stages of the discharging process goes from 1:6 in fully charged conditions to 1:12, 1:24, etc., until the lithium is almost fully removed from the graphitic layers [32]. As a consequence, the anodic potential increases in discrete steps and reaches a maximum when the battery is fully discharged [31]. In other cases, the phase transition is a continuous process that does not produce any noticeable discontinuity in the electrode potential, which appears as a smooth S-shaped curve, as in Figure 1c. This is the case of most cobalt-based electrodes, as in the so-called NMC batteries, which use mixed metal oxides of lithium, nickel, manganese and cobalt as a cathode.

The resulting cell voltage is a combination of the potentials of both the anode and cathode, and so the individual effects of the three behaviors illustrated in Figure 1 tend to blend together and contaminate each other. However, since the anodic potential is typically an order of magnitude lower than the cathodic potential, the overall voltage profile is expected to be predominantly influenced by the characteristics of the cathode material.

2.2. Open Circuit Voltage Modeling

As already pointed out, semi-empirical expressions are very popular in modeling the open circuit voltage of Li-ion batteries because of their simplicity. In particular, the approach adopted in [24,25] has gained attention among researchers since it allows an easy estimation of the unknown parameters without the need for non-linear model optimization methods. According to this approach, and by omitting the effect of the current, the open circuit voltage as a function of the transferred charge q can be expressed as

$$V_{oc}(q) = E_o - K\left(\frac{Q}{Q-q}\right)q + Ae^{-Bq} \tag{2}$$

where Q is the total battery capacity, and E_0, K, A and B are empirical constants that can be readily calculated based on specific features of the experimental discharge curve. The model appears very accurate when describing batteries whose voltage is controlled mainly by first order phase transitions, i.e., similar to the one in Figure 1a, where the plateau voltage E_0 in Equation (2) is corrected near fully charged conditions by the positive exponential term and near fully discharged conditions by a hyperbolic negative term. However, the application to batteries with non-flat characteristic curves appears more challenging since the exponential and hyperbolic regions are more difficult to identify and may overlap.

In this paper, an alternative semi-empirical approach has been proposed to address V_{oc} in batteries with quasi-continuous or continuous solid phase transformations (Figure 1b,c). This approach aims to maintain a closer connection to the actual chemical processes occurring during battery operation while avoiding, at the same time, overcomplexity and the need for extensive solid phase characterization efforts. In order to cope with the complications of solid state thermodynamics in the presence of multiple phases, especially when referring to commercial batteries whose exact materials and chemistry may not be fully known, the scenario depicted in Section 2.1 is simplified here by assuming a single generic lithiated compound at the anode, Li_xA, and a single generic lithiated compound at the cathode, Li_yC, where A and C indicate the non-lithiated forms of the anodic and cathodic materials, respectively. This is equivalent to considering the electrodes as two solid solutions with variable concentration of such species in a way to reproduce the same open circuit voltage observed in the actual cell. To this goal, the two semi-reactions are written for each transferred cation as

$$\alpha \mathrm{Li}_x\mathrm{A} \rightleftharpoons \alpha\mathrm{A} + \mathrm{Li}^+ + \mathrm{e}^-$$
$$\beta\mathrm{C} + \mathrm{Li}^+ + \mathrm{e}^- \rightleftharpoons \beta\mathrm{Li}_y\mathrm{C}$$

where the unknown stoichiometric coefficients $\alpha = 1/x$ and $\beta = 1/y$ are introduced to provide the model with two adjustable parameters. The overall reaction becomes

$$\alpha \mathrm{Li}_x\mathrm{A} + \beta\mathrm{C} \rightleftharpoons \alpha\mathrm{A} + \beta\mathrm{Li}_y\mathrm{C} \tag{3}$$

Since the lithiated anodic and cathodic reactants have been defined only in generic terms, the main idea behind the proposed model is to describe their unknown chemical potentials μ_i by relating them to the chemical potentials $\mu_{i,fc}$ observed in fully charged conditions and at the same temperature. To this goal, thermodynamic activities a_i are introduced according to their classical definition:

$$\mu_i - \mu_{i,fc} = RT\ln a_i \tag{4}$$

where R is the universal gas constant (8.314 J mol^{-1} K^{-1}), and T is the absolute temperature (K), and the difference between the Gibbs free energy change in the overall reaction in current and fully charged conditions is, therefore,

$$\Delta g_r - \Delta g_{r,fc} = \sum \nu_i(\mu_i - \mu_{i,fc}) = \beta RT\ln a_{\mathrm{Li}_y\mathrm{C}} - \alpha RT\ln a_{\mathrm{Li}_x\,\mathrm{A}} \tag{5}$$

where ν_i is the generic stoichiometric coefficient (taken positive for products and negative for reactants) and where the activities of non-lithiated solids have been assumed to be equal to one. The activities of solid lithium at the two electrodes are expressed as the ratio of the current and the reference content (in fully charged conditions) of the lithiated species:

$$a_{\mathrm{Li}_x\mathrm{A}} = \frac{Q_A - q}{Q_A} \tag{6}$$

$$a_{\mathrm{Li}_y\mathrm{C}} = \frac{Q_C - Q + q}{Q_C - Q} \tag{7}$$

where Q is the amount of lithium corresponding to the battery total capacity, q is a measure of the transferred lithium ions starting from fully charged conditions (so that $0 \le q \le Q$), Q_A and Q_C are the total amounts of lithium at the anode and cathode, respectively, which leads to $Q \le \min(Q_A, Q_C)$. By bringing Equations (1), (6) and (7) into Equation (5), and after introducing the state of charge (SoC) of the batter, y defined as

$$SoC = \frac{Q - q}{Q} \tag{8}$$

one obtains

$$V_{oc} = V_{oc,fc} - \frac{RT}{F}\ln\left[\frac{\lambda - SoC}{\lambda - 1}\right]^{\alpha}\left[\frac{\delta\lambda - 1 + SoC}{\delta\lambda}\right]^{-\beta} \tag{9}$$

where $\lambda = Q_C/Q$ and $\delta = Q_A/Q_C$.

In conclusion, Equation (9) represents the Nernst equation for the battery open circuit voltage when taking the fully charged conditions as reference. It can be verified that $V_{oc} = V_{oc,fc}$ when $SoC = 1$, while the condition $SoC = 0$ provides the cut-off voltage.

2.3. Equivalent Circuit Model

In order to describe the battery load voltage V_b under operational conditions, the open circuit voltage needs to be corrected by a term accounting for the dissipative effects of the current I, which reduces the available theoretical voltage during discharging. To this goal, the linear term $R_{eq}I$ is subtracted from the open circuit voltage:

$$V_b = V_{oc} - R_{eq}I \tag{10}$$

which corresponds to the adoption of a classical equivalent circuit model (ECM) widely used in similar studies [29]. In this basic ECM, the electromotive force generated by the battery is in series with an equivalent internal resistance R_{eq}, which accounts for the impedance of the real battery and concentrates all possible causes of energy dissipation (ohmic dissipation, kinetic barriers, mass transfer limitations, etc.). More advanced ECMs may include additional resistances and capacitors to account for a dynamic response due to rapid changes in the current [27,30], but these effects are omitted here.

Battery self-discharge and dissipative heating are neglected, and the model is applied at a constant temperature. Moreover, the model cannot predict battery aging but is expected to describe the voltage-capacity characteristics at any battery age in all those cases where the actual capacity Q can be adjusted according to the number of cycles. Equation (10) can describe the voltage also during charging by reversing the sign of the current from positive to negative. This transforms the $-R_{eq}I$ term into an additive amount that increases the overall voltage and, hence, the energy provided to the device compared to the energy retrieved during discharging.

3. Results and Discussion

The accuracy of the proposed model is evaluated by predicting the voltage in two commercial batteries of the 18,650 type (18 mm in diameter, 65 mm in length, cylindrical), each characterized by distinct cathode materials and capacity. This battery format is particularly widespread as most battery packs in both stationary and mobile applications are assembled from individual cells of this type. The first battery considered in this work is the Panasonic CGR18650AF, with a cathode made of lithium nickel cobalt manganese oxide ($LiCoNiMnO_2$ or NMC) and a maximum standard capacity (evaluated at specific conditions defined by the manufacturer) of 2050 mAh. The second battery is the Panasonic NCR18650B, with a cathode made of lithium cobalt nickel aluminum oxide ($LiCoNiAlO_2$ or NCA) and a standard maximum capacity of 3350 mAh. The relevant discharge curves at various constant currents are reproduced in Figure 2, as extracted from the manufacturer's datasheets [33,34]. Three different sets of data are available for the first battery at three different currents (0.39, 1.95 and 3.9 A, corresponding to 0.2 C, 1 C and 2 C, respectively), while voltage curves for the second battery refer to four different constant currents (0.67, 1.675, 3.35 and 6.7 A, or 0.2 C, 0.5 C, 1 C and 2 C, respectively). The maximum available capacity of the batteries under real operational conditions, to be used to determine the SoC in Equation (8), has been considered as dependent on the current and has been read from the available discharge curves; the relevant values are reported in Table 1 and correspond to the energy extracted when going from fully charged conditions to the cut-off voltage of 2.5 V for both batteries. According to the Peukert effect, this maximum capacity decreases when the discharge current increases, although other effects could also influence its value, such as the conditions under which the last charging and the discharging were carried out or the age of the battery (maximum capacity usually decreases with age but an increase may also be observed during early cycling [35]). As a consequence, discharge curves crossing at low SoC is not rare, as observed in Figure 2b in the case of NCR18650B.

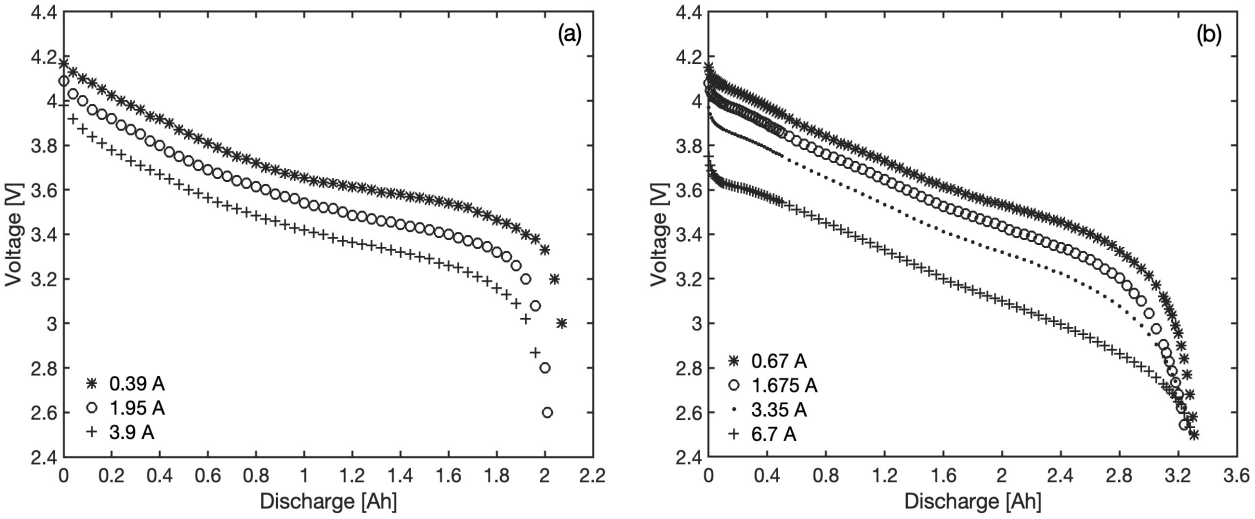

Figure 2. Characteristics discharge curves at 25 °C and different currents for (**a**) CGR18650AF and (**b**) NCR18650B.

Table 1. Panasonic battery specifications and model parameters.

Symbol	Description	Units	CGR18650AF	NCR18650B
	Standard capacity	mAh	2050	3350
$V_{oc,fc}$	Voltage at fully charged conditions	V	4.19	4.20
I	Current	A	0.39, 1.95, 3.9	0.67, 1.675, 3.35, 6.7
Q	Observed capacity at each current	mAh	2070, 2010, 1960	3310, 3240, 3280, 3280
a	Parameter in Equation (11)	mΩ	−14.82	−8.64
b	Parameter in Equation (11)	mΩ	72.69	72.61
α	Stoichiometric coefficient at anode	-	10.14	11.12
β	Stoichiometric coefficient at cathode	-	2.55	6.69
λ	Q_C/Q	-	1.10	1.14
δ	Q_A/Q_C	-	0.91	0.88

3.1. Equivalent Internal Resistance

With reference to the general form of the model as in Equation (10), the effect of the current is actually isolated in one linear term, $R_{eq}I$. A plot of the battery voltage versus the current can be extracted from the available discharge curves at constant *SoC* values, as reported in Figure 3, which confirms that any deviation from linearity in the voltage versus current relationships is modest and mostly limited to very low *SoC* values of the second battery. In particular, the observed linearity suggests that ohmic-like losses dominate over the considered current range and that typical causes of non-linearity, such as the overpotential produced by mass transfer limitations at high currents, do not onset at the considered C-rates. Moreover, these plots also allow a direct estimation of the equivalent resistance as the slope of the best fitting lines. The estimates of R_{eq} at different states of charge are plotted in Figure 4, revealing values in the range 60–75 mΩ. These values show a slight and fairly linear decreasing trend when moving towards fully charged conditions. This effect, even if modest, has been taken into account in the model in particular to improve the accuracy of the voltage predictions at very low *SoC*, where the sensitivity to the model parameters is highest. To this goal, the equivalent resistance is expressed as

$$R_{eq} = a \cdot SoC + b \tag{11}$$

and the corresponding best fit parameters are given in Table 1.

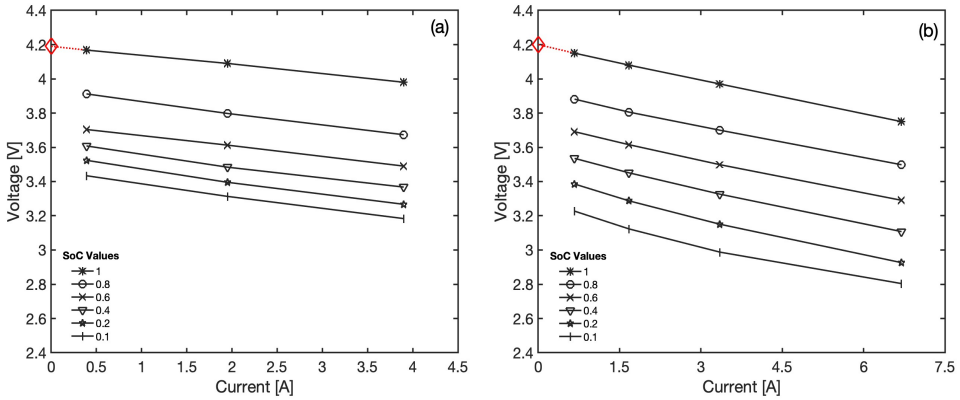

Figure 3. V_b versus I curves at constant *SoC* for (**a**) CGR18650AF, (**b**) NCR18650B, and extrapolation to $I = 0$ for estimation of $V_{oc,fc}$. Red diamonds indicate $V_{oc,fc}$ for the two batteries.

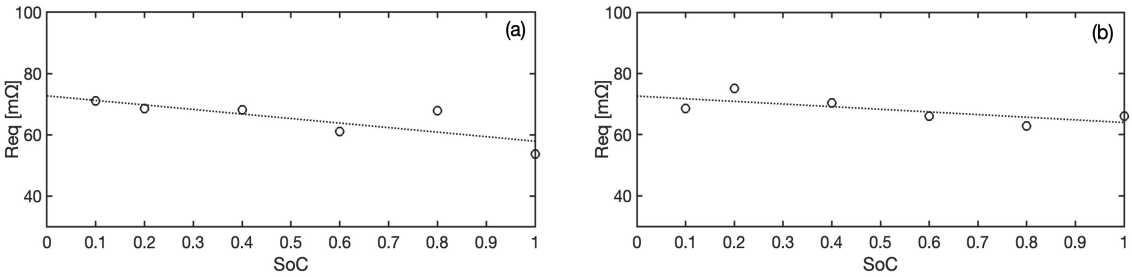

Figure 4. Equivalent resistance at different *SoC* for (**a**) CGR18650AF and (**b**) NCR18650B. Empty circles denote the estimates of R_{eq} from experimental $V - I$ data and dotted lines denote the interpolating models according to Equation (11).

3.2. Fully Charged Open Circuit Voltage

From Figure 3, it is possible to obtain a reasonable estimation of the open circuit voltage in fully charged conditions by linearly extrapolating the voltage at $SoC = 1$ until it intercepts the vertical axis at zero current. The extracted values, 4.19 V and 4.20 V, respectively, are similar and in line with what should be expected from classic Li-ion based electrode pairs. In the lack of direct observations, this approach assumes that the linear trends shown in Figure 3 hold until zero currents, hence, neglecting possible non-linear phenomena and voltage gaps reported at near zero currents [36].

3.3. Model Fitting Results

After extracting the values of the internal equivalent resistance R_{eq} and of the open circuit voltage in fully charged conditions directly from the discharge curves, the model presents four more adjustable parameters: the stoichiometric coefficients α and β and the parameters λ and δ, accounting for the relationships among the maximum amounts of lithium at the electrodes and the battery total capacity. These are estimated through an optimization process that minimizes, for each battery, the sum of all absolute errors between model predictions and measured voltage by means of a non-linear generalized reduced gradient algorithm. The comparison between the actual discharge curves and the best-fit model predictions is shown in Figure 5 for both batteries and all available constant current datasets, as a function of the *SoC*.

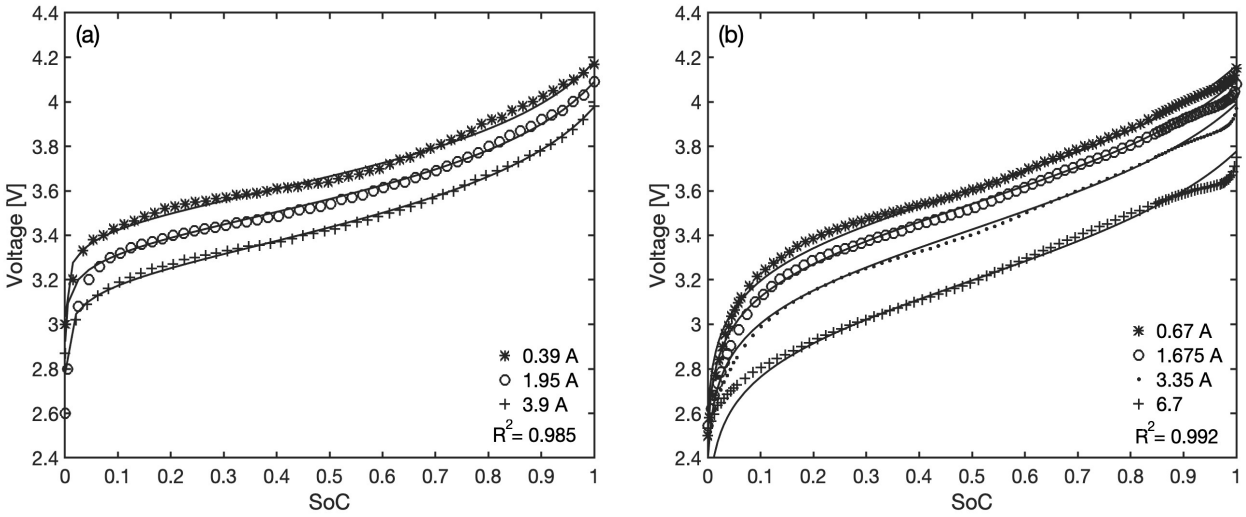

Figure 5. Fitting results for battery discharge curves of (**a**) CGR18650AF and (**b**) NCR18650B (continuous lines indicate model predictions).

The model generally shows a good level of accuracy over the entire discharging range, with overall coefficients of determination R^2 equal to 0.985 and 0.992, respectively. The val-

ues of the best-fit parameters for each battery are reported in Table 1. The two stoichiometric coefficients are both positive, confirming that the type of effect of the anode and cathode potential change during discharging is correctly predicted by Equation (9), and since $\alpha > \beta$, the potential variation at the anode tends to dominate the shape of the overall voltage drop. The values of γ and δ are always close to one, and this is also consistent with their definitions; in particular, since $\delta < 1$, the maximum amount of virtual lithiated compound at the anode is estimated to be slightly less than at the cathode.

The region revealing the highest discrepancies between the observed voltage and predictions is the one at low *SoC* values, and this is particularly evident when referring to the residual errors in Figure 6, reported separately for each set of data. Two main reasons could be behind this. On one hand, there are difficulties in extracting an accurate estimation of the maximum available capacity for each current, due to some of the discharge curves of the second battery crossing each other near full depletion conditions. Such uncertainties produce a larger relative error at low *SoC* values in the light of Equation (8). On the other hand, the linear increase adopted for the internal resistance of these two batteries may not be sufficient to take into account the dissipative phenomena taking place near battery depletion, suggesting that non linear correlations for R_{eq} may benefit (at least numerically) the model accuracy in this region; this aspect is addressed in more detail in Section 3.5. For the rest of the *SoC* range, clear patterns can be observed in the residuals, which fluctuate in a rather predictable way around zero (overall mean residual error is $-3.2 \times 10^{-3} \pm 0.033$ V and $2.45 \times 10^{-3} \pm 0.039$ V, respectively). This is certainly a reflection of the discrete jumps in the chemical activities of the electrode materials in real batteries due to phase transitions, whereby the nature of the proposed model denies such discontinuities and provides for a smoothing of the voltage curves. The largest errors caused by these simplifications are found in the initial discharge stages of the NCR18650B battery (see residuals at low *SoC* in Figure 6b), and in particular, this can be attributed to the solid phase activity in the anodic lithiated graphite at the start of the discharging process [35].

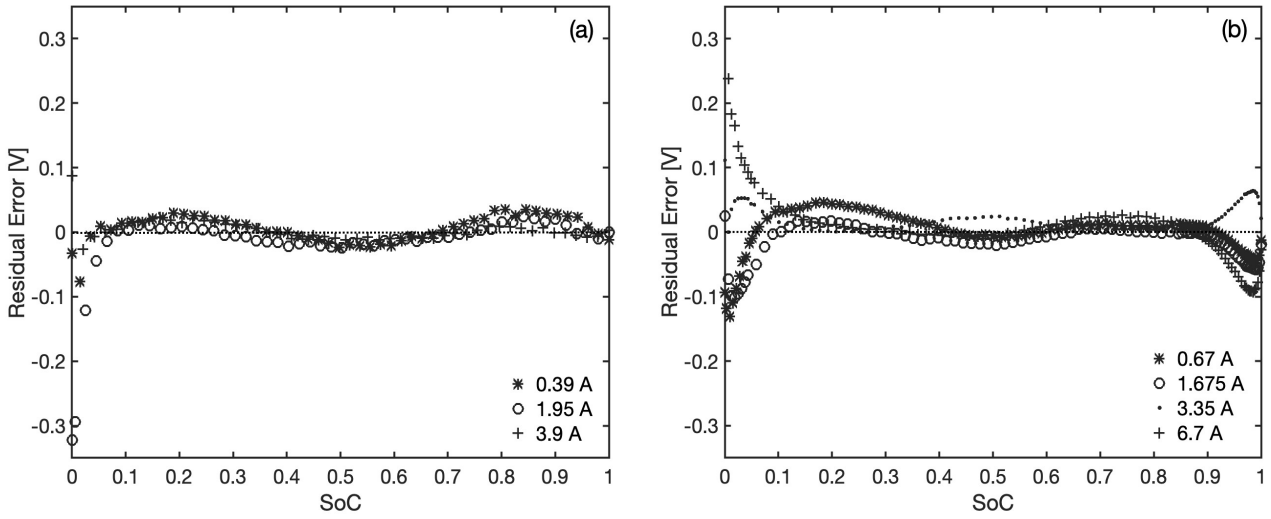

Figure 6. Residual errors of battery discharge curves for (**a**) CGR18650AF and (**b**) NCR18650B.

3.4. Model Reduction

Based on the best-fit parameter values reported in Table 1, it can be observed that for both batteries, it is $\lambda\delta \approx 1$ or $Q_A \approx Q$, indicating that the anode is the limiting electrode for the total capacity so that there is nearly no lithium left at the anode at the end of the discharging phase. This is not necessarily a general result and does not necessarily reflect what happens in real batteries, and lacking external information on the quantitative composition of the electrodes, it is considered here merely as a numerical outcome. Based

on this result, however, a useful simplification can be introduced in Equation (9) without a significant loss in model accuracy:

$$V_{oc} = V_{oc,fc} - \frac{RT}{F}\ln\left[\frac{\lambda - SoC}{\lambda - 1}\right]^{\alpha} SoC^{-\beta} \tag{12}$$

which corresponds to reducing the actual number of parameters from 4 to 3.

This model reduction introduces a minor theoretical inconsistency, i.e., the activity at the anode becomes zero already at the cut-off voltage, as can be verified in Equation (6) by putting $q = Q$ (from $SoC = 0$) and $Q = Q_A$ (from $\lambda\delta = 1$), causing the battery voltage to approach negative infinity. This is a consequence of the nearly infinite slope of the voltage curves near battery depletion and the consequent difficulty for the model to discriminate between cut-off capacity and zero voltage capacity. This inconsistency is not expected to have practical consequences, since the battery operation beyond the cut-off voltage is usually irrelevant but requires the exclusion of the cut-off voltage condition during the non-linear optimization of the reduced model, as this would otherwise produce an infinite error.

3.5. Charging and Discharging Cycle

To test the model performance through a full charge–discharge cycle, the Tesla 4680 battery cell was considered. Designed by Tesla for use in their own electric vehicles and stationary energy storage systems, this cell has a total capacity of 23.35 Ah and is at the forefront of the current technological developments in the Li-ion battery sector. The materials used for the electrodes are lithiated graphite at the anode and nickel manganese cobalt (NMC) oxide at the cathode [37]. For the voltage characteristic curves during charging and discharging as a function of the battery charge, the ones obtained at a constant current of 2.5 A at the Laboratory for Energy Storage and Conversion, University of California San Diego, and made available in [38] have been used; these are shown in Figure 7a.

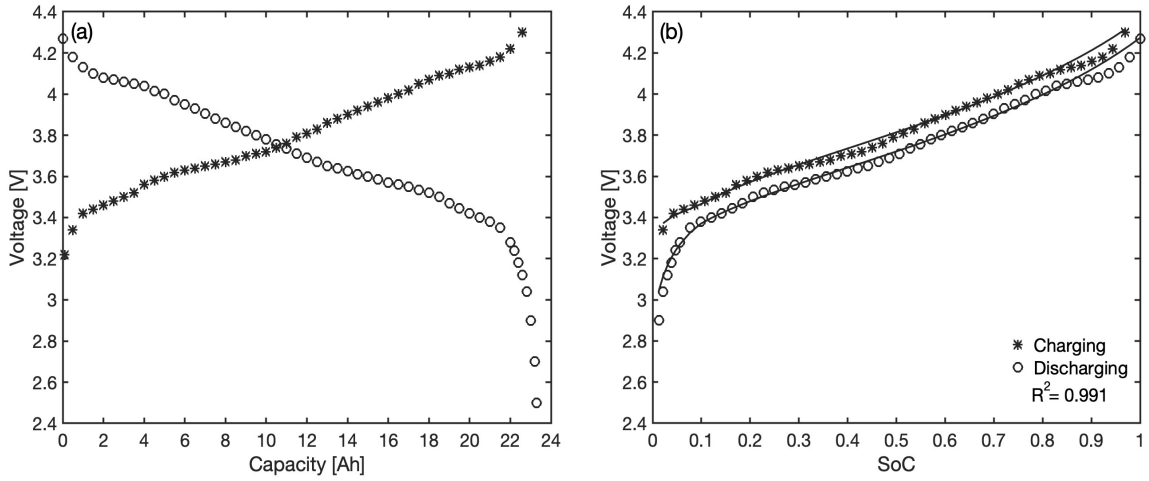

Figure 7. Voltage curves for Tesla 4680 at 2.5 A: (**a**) Charging and discharging curves versus transferred charge [38], (**b**) model predictions and observed voltage versus *SoC*.

This allows for an estimation of the internal resistance at different *SoC* values as a function of the measured voltage difference ΔV_b between charging and discharging, considering that V_{oc} is invariant to the current, and, by means of Equation (10), we obtain

$$\Delta V_b(SoC) = 2R_{eq}|I| \tag{13}$$

where the absolute value of I must be used. The resulting R_{eq} is shown in Figure 8, where it oscillates in most of the *SoC* range without a clear trend, so that the average value of 18.6 mΩ can be considered to be representative. However, the abrupt increase at

$SoC < 0.1$ is not to be neglected if good model accuracy is also required in that range (such range is often avoided by real battery operation in order to preserve battery life, but its accurate prediction still significantly contributes to the effectiveness of the EMS). Therefore, the internal equivalent resistance will be expressed here as

$$R_{eq}\ [\mathrm{m}\Omega] = \begin{cases} 18.6 & \text{if } SoC \geq 0.1 \\ -12538SoC^3 + 6482SoC^2 - 1049SoC + 71.20 & \text{if } SoC < 0.1 \end{cases} \quad (14)$$

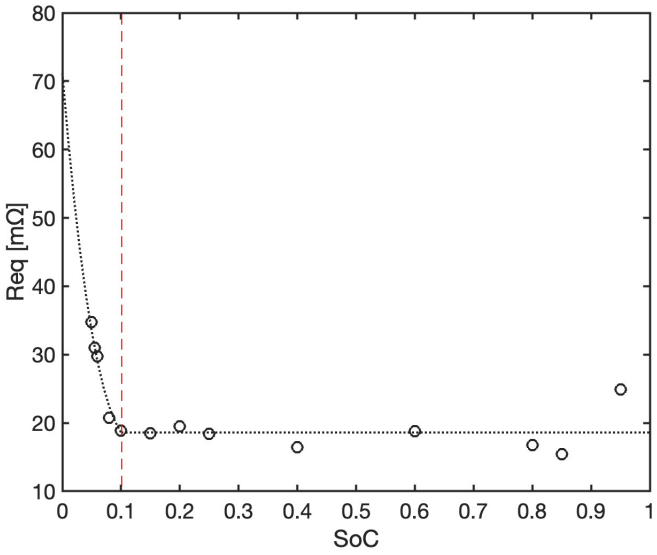

Figure 8. Equivalent resistance at different SoC for Tesla 4680. Empty circles denote the estimates of R_{eq} from experimental $V - I$ data and dotted black lines denote the interpolating models according to Equation (14), with the threshold of $SoC = 0.1$ indicated by the red dashed line.

The plateau value of 18.6 mΩ is on the lower end of the typical impedance values expected for a Li-ion battery, but the general trend is consistent with what has been found experimentally in direct measurement campaigns of the internal pulse resistance carried out on the Tesla 4680 cell [37], where a sharp increase is also observed near fully discharged conditions.

The open circuit voltage at fully charged conditions, $V_{oc,fc}$, can be estimated in the light of Equation (10) and of the plateau value of the equivalent resistance found earlier:

$$V_{oc,fc} = V_{fc} + R_{eq}I = 4.32\ \mathrm{V} \quad (15)$$

where $V_{fc} = 4.27$ V is the voltage at $SoC = 1$ during discharge, and $I = 2.5$ A is the applied current.

The open circuit voltage has been described by applying the reduced version of the model (Equation (12)), following preliminary tests that also revealed, in this case, no significant loss in accuracy compared to the full model (Equation (9)). To this goal, and as discussed in Section 3.4, the voltage data at $SoC = 0$ have been disregarded during the optimization procedure, both during charging and discharging.

The comparison between observed voltage and model predictions is reported as a function of the SoC in Figure 7b for both charging and discharging phases. A very good level of overall accuracy is reached ($R^2 = 0.991$) by using the following best-fit parameters: α = 18.31, β = 3.69 and λ = 1.28. The parameter values are reasonably aligned with the two previous batteries; however, no straightforward conclusions can be drawn from their comparison since they mostly reflect intensive electrode properties (α and β are stoichiometric ratios, and λ is a capacity ratio) and are, therefore, affected in a way difficult to predict by differences in the materials used and the overall technologies employed (the

Tesla battery, for example, benefits from much more recent developments in the sector compared to the Panasonic batteries).

The overall mean residual error is -0.0117 ± 0.0316 V and the large prediction errors observed at low *SoC* for the Panasonic batteries are now absent, confirming that the choice of a non-linear correlation for R_{eq} adequately absorbs the model limitations in this range and greatly improves the local accuracy. On the other side, the error at *SoC* approaching one due to material phase transitions in the electrodes remains evident for both the discharging and the charging curves. This is expected as it mostly stems from the inability of the proposed model to describe individual phase transformations in the electrodes.

4. Conclusions

This paper presents a novel approach for estimating the voltage versus the state of charge of a Li-ion battery, primarily intended for batteries with second order phase transformations where other popular semi-empirical approaches for open circuit voltage modeling may not be easily applicable. The general aim of this investigation is to contribute to the enhancement of energy management systems in mobility and stationary energy storage systems, as in residential microgrids with energy production from renewable sources. The accurate prediction of the battery *SoC* based on voltage measurements is considered a crucial feature in these systems.

The proposed model is based on the classical Nernst equation to describe the continuous change in the open circuit voltage during charging and discharging. All remaining effects and uncertainties are lumped into one linear term representing energy dissipations under load conditions. The model calibration is based on data usually made available from the manufacturer's datasheets or from voltage measurements, without the need for material characterization efforts.

The model has been applied to describe two Panasonic cylindrical cells in order to test its ability to correctly predict the voltage under different current loads and to the Tesla 4680 battery cell to describe a full charge–discharge cycle. All tested batteries have cobalt-containing cathodes, although with different compositions and capacities. In all three cases, the fit appears to be good quality with R^2 values above 0.98, and the model is able to catch and correctly reproduce all main features of the voltage curves. Considerations on the values of the best fit parameters suggest a possible reduction in the complexity of the model, with the number of unknown parameters reduced from 4 to 3.

Major deviations between model predictions and observed values only onset at very high and very low *SoC* values. These are mostly due to the model not accounting for individual phase transformations in the electrodes (in the first case) and uncertainties in the estimation of the equivalent internal resistance at a very low charging state (in the second case), although other unaccounted for phenomena may contribute as well.

Furthermore, the applicability of the proposed model to batteries with cathodic materials not containing cobalt, particularly LFP type batteries and all those characterized by a main voltage plateau, remains unexplored at the time of writing and may require specific adjustments to take into account the different solid phase thermodynamics.

Author Contributions: Conceptualization and methodology, A.A., M.I. and A.D.; software, A.A.; formal analysis, M.I.; writing—original draft preparation, A.A.; writing—review and editing, A.A., M.I. and A.D.; supervision, M.I. and A.D. All authors have read and agreed to the published version of the manuscript.

Funding: This work was funded by the Next Generation EU—Italian NRRP, Mission 4, Component 2, Investment 1.5, call for the creation and strengthening of 'Innovation Ecosystems', building 'Territorial R&D Leaders' (Directorial Decree n. 2021/3277)—project Tech4You—Technologies for climate change adaptation and quality of life improvement, n. ECS0000009. This work reflects only the authors' views and opinions; neither the Ministry for University and Research nor the European Commission can be considered responsible for them.

Conflicts of Interest: The authors declare no conflicts of interest.

Abbreviations

The following abbreviations are used in this manuscript:

ECM	Equivalent circuit model
EIM	Electrochemical impedance model
EM	Electrochemical model
EMS	Energy management system
LFP	Lithium iron phosphate
NCA	Nickel cobalt aluminum
NMC	Nickel manganese cobalt
RUL	Remaining useful life
SoC	State of charge
SoH	State of health

References

1. Hasib, S.A.; Islam, S.; Chakrabortty, R.K.; Ryan, M.J.; Saha, D.K.; Ahamed, H.; Moyeen, S.I.; Das, S.K.; Ali, F.; Islam, R.; et al. A Comprehensive Review of Available Battery Datasets, RUL Prediction Approaches, and Advanced Battery Management. *IEEE Access* **2021**, *9*, 86166–86193. [CrossRef]
2. Elmahallawy, M.; Elfouly, T.; Alouani, A.; Massoud, A.M. A Comprehensive Review of Lithium-Ion Batteries Modeling, and State of Health and Remaining Useful Lifetime Prediction. *IEEE Access* **2022**, *10*, 119040–119070. [CrossRef]
3. Zhao, J.; Zhu, Y.; Zhang, B.; Liu, M.; Wang, J.; Liu, C.; Hao, X. Review of State Estimation and Remaining Useful Life Prediction Methods for Lithium-Ion Batteries. *Sustainability* **2023**, *15*, 5014. [CrossRef]
4. Wang, Y.; Zuo, X. State of Charge Estimation Methods and Application Scenarios of Lithium-Ion Batteries. *Power Syst. Autom.* **2022**, *46*, 193–207.
5. Selvaraj, V.; Vairavasundaram, I. A comprehensive review of state of charge estimation in lithium-ion batteries used in electric vehicles. *J. Energy Storage* **2023**, *72*, 108777. [CrossRef]
6. He, L.; Hu, M.; Shi, Q.; Ye, W. A staged state of charge estimation algorithm for lithium-ion batteries. *Power Electron. Technol.* **2020**, *54*, 8–11.
7. Li, C.; Xiao, F.; Fan, Y.; Yang, G.; Tang, X. State of Charge Estimation of Lithium Ion Battery Based on Gated Cyclic Unit Neural Network and Huber-M Estimation Robust Kalman Filter Fusion Method. *J. Electr. Technol.* **2020**, *35*, 2051–2062.
8. Wang, X.; Zheng, C.; Zhang, S.; Dai, M.; Xiao, W.; Chen, X. Summary of fusing algorithm research in estimation for state of charge of battery. *Sichuan Electr. Power Technol.* **2021**, *44*, 43–46.
9. Wu, L.; Pang, H.; Jin, J.; Geng, Y.; Liu, K. A Review of State of Charge Estimation Methods for Lithium Ion Batteries Based on Electrochemical Models. *J. Electr. Technol.* **2022**, *37*, 1703–1725.
10. Wu, C.; Hu, W.; Meng, J.; Liu, Z.; Cheng, D. State of Charge Estimation of Lithium Ion Battery Based on Maximum Correlation Entropy Extended Kalman Filter Algorithm. *J. Electr. Technol.* **2021**, *36*, 5165–5175.
11. Schmidt, A.P.; Bitzer, M.; Imre, Á.W.; Guzzella, L. Experiment-driven electrochemical modeling and systematic parameterization for a lithium- ion battery cell. *J. Power Sour.* **2010**, *195*, 5071–5080. [CrossRef]
12. Rahimian, S.K.; Rayman, S.; White, R.E. State of charge and loss of active material estimation of a lithium ion cell under low earth orbit condition using Kalman filtering approaches. *J. Electrochem. Soc.* **2012**, *159*, A860. [CrossRef]
13. Schmitt, J.; Horstkötter, I.; Bäker, B. Electrical lithium-ion battery models based on recurrent neural networks: A holistic approach. *J. Energy Storage* **2023**, *58*, 106461. [CrossRef]
14. Krishnamoorthy, U.; Gandhi Ayyavu, P.; Panchal, H.; Shanmugam, D.; Balasubramani, S.; Al-rubaie, A.J.; Al-khaykan, A.; Oza, A.D.; Hembrom, S.; Patel, T.; et al. Efficient Battery Models for Performance Studies-Lithium Ion and Nickel Metal Hydride Battery. *Batteries* **2023**, *9*, 52. [CrossRef]
15. Çorapsiz, M.R.; Kahveci, H. A study on Li-ion battery and supercapacitor design for hybrid energy storage systems. *Energy Storage* **2023**, *5*, e386. [CrossRef]
16. Shin, J.; Kim, W.; Yoo, K.; Kim, H.; Han, M. Vehicular level battery modeling and its application to battery electric vehicle simulation. *J. Power Sources* **2023**, *556*, 232531. [CrossRef]
17. Navas, S.J.; González, G.C.; Pino, F.; Guerra, J. Modelling Li-ion batteries using equivalent circuits for renewable energy applications. *Energy Rep.* **2023**, *9*, 4456–4465. [CrossRef]
18. Quelin, A.; Damay, N. Coupling electrical parameters of a battery equivalent circuit model to electrodes dimensions. *J. Power Sources* **2023**, *561*, 232690. [CrossRef]
19. Tran, M.K.; DaCosta, A.; Mevawalla, A.; Panchal, S.; Fowler, M. Comparative study of equivalent circuit models performance in four common lithium-ion batteries: LFP, NMC, LMO, NCA. *Batteries* **2021**, *7*, 51. [CrossRef]
20. Bibin, C.; Vijayaram, M.; Suriya, V.; Ganesh, R.S.; Soundarraj, S. A review on thermal issues in Li-ion battery and recent advancements in battery thermal management system. *Mater. Today Proc.* **2020**, *33*, 116–128. [CrossRef]

21. Tran, M.K.; Mathew, M.; Janhunen, S.; Panchal, S.; Raahemifar, K.; Fraser, R.; Fowler, M. A comprehensive equivalent circuit model for lithium-ion batteries, incorporating the effects of state of health, state of charge, and temperature on model parameters. *J. Energy Storage* **2021**, *43*, 103252. [CrossRef]
22. Zhang, R.; Xia, B.; Li, B.; Cao, L.; Lai, Y.; Zheng, W.; Wang, H.; Wang, W.; Wang, M. A Study on the Open Circuit Voltage and State of Charge Characterization of High Capacity Lithium-Ion Battery Under Different Temperature. *Energies* **2018**, *11*, 2408. [CrossRef]
23. Shepherd, C.M. Design of Primary and Secondary Cells—Part 2. An equation describing battery discharge. *J. Elec. Soc.* **1965**, *112*, 657–664. [CrossRef]
24. Tremblay, O.; Dessaint, L.-A.; Dekkiche, A.-I. A Generic Battery Model for the Dynamic Simulation of Hybrid Electric Vehicles. In Proceedings of the 2007 IEEE Vehicle Power and Propulsion Conference, Arlington, TX, USA, 9–12 September 2007; pp. 284–289.
25. Tremblay, O.; Dessaint, L.-A. Experimental Validation of a Battery Dynamic Model for EV Applications. *Wor. Electr. Veh. J.* **2009** *3*, 289–298. [CrossRef]
26. Matlab/Simulink Libraries: Generic Battery Model. Available online: https://www.mathworks.com/help/sps/powersys/ref/battery.html (accessed on 21 March 2024).
27. Binelo, M.F.; Sausen, A.T.; Sausen, P.S.; Binelo, M.O.; Campos, M. Multi-phase method of estimation and adaptation of parameters of Electrical Battery Models. *Int. J. Energy Res.* **2020**, *45*, 1023–1037. [CrossRef]
28. Cabello, J.M.; Bru, E.; Roboam, X.; Lacressonnière, F.; Junco, S. Battery dynamic model improvement with parameters estimation and experimental validation. In Proceedings of the 8th International Conference on Integrated Modeling and Analysis in Applied Control and Automation, Bergeggi, Italy, 21–23 September 2015.
29. Campagna, N.; Castiglia, V.; Miceli, R.; Mastromauro, R.A.; Spataro, C.; Trapanese, M.; Viola, F. Battery Models for Battery Powered Applications: A Comparative Study. *Energies* **2020**, *13*, 4085. [CrossRef]
30. Potrykus, S.; Kutt, F.; Nieznański, J.; Fernandez Morales, F. J. Advanced Lithium-Ion Battery Model for Power System Performance Analysis. *Energies* **2020**, *13*, 2411. [CrossRef]
31. Huggins, R.A. *Advanced Batteries: Materials Science Aspects*, 1st ed.; Springer: New York, NY, USA; Department of Materials Science and Engineering, Stanford University: Stanford, CA, USA, 2009; pp. 30–36.
32. Li, W.-B.; Lin, S.-Y.; Lin, M.-F.; Lin, K.-I. Essential Electronic Properties of Stage-1 Li/Li+-Graphite-Intercalation Compounds for Different Concentrations. *Condens. Matter* **2022**, *7*, 35. [CrossRef]
33. Panasonic CGR18650AF Battery Datasheet. Available online: https://www.datasheets.com/part-details/cgr18650af-panasonic-31361744$#$datasheet (accessed on 25 May 2024).
34. Panasonic NCR18650B Battery Datasheet. Available online: https://www.imrbatteries.com/content/panasonic_ncr18650b-2.pdf (accessed on 30 April 2024).
35. Guo, J.; Li, Y.; Meng, J.; Pedersen, K.; Gurevich, L.; Stroe, D.-I. Understanding the mechanism of capacity increase during early cycling of commercial NMC/graphite lithium-ion batteries. *J. Energy Chem.* **2022**, *74*, 34–44. [CrossRef]
36. Dreyer, W.; Jamnik, J.; Guhlke, C.; Huth, R.; Moškon, J.; Gaberšcek, M. The thermodynamic origin of hysteresis in insertion batteries. *Nat. Mater.* **2010**, *9*, 448–453. [CrossRef]
37. Ank, M.; Sommer, A.; Abo Gamra, K.; Schöberl, J.; Leeb, M.; Schachtl, J.; Streidel, N.; Stock, S.; Schreiber, M.; Bilfinger, P.; et al. Lithium-Ion Cells in Automotive Applications: Tesla 4680 Cylindrical Cell Teardown and Characterization. *J. Electrochem. Soc.* **2023**, *170*, 120536. [CrossRef]
38. Battery Design: Tesla 4680 Cell. Available online: https://www.batterydesign.net/tesla-4680-cell/ (accessed on 12 July 2024).